Ultrasonic Properties and Morphology of Devulcanized Rubber Blends

Shui-Han Zhu,[1] Alexander Penlidis,[1] Costas Tzoganakis,[1] Ed Ginzel[2]

[1]*Institute for Polymer Research, Department of Chemical Engineering, University of Waterloo, Canada N2L 3G1*
[2]*Materials Research Institute, Waterloo, Ontario, Canada N2J 4G8*

Received 11 January 2011; accepted 11 July 2011
DOI 10.1002/app.35251
Published online 25 October 2011 in Wiley Online Library (wileyonlinelibrary.com).

ABSTRACT: The ultrasonic properties of two devulcanized rubber (DR) blends with a styrene-butadiene-styrene (SBS) copolymer compound (ACE) are investigated using a transmission method. The DR materials are obtained from commercial rubber crumbs (RC) by a proprietary devulcanization technique. Measurements on the acoustic attenuation and travel velocity are conducted on the samples with different sample thicknesses in the pulsed mode. Attenuation coefficients of the materials are obtained by changing the frequency of the ultrasound in the tuned tone-burst mode. The two DR/ACE blends show marked differences in the attenuation and attenuation coefficient, although the ultrasonic velocities are similar. These differences arise from the variation of the remaining degree of crosslinking in the DR materials. The acoustic velocities in the three materials are similar. The morphologies of the DR/ACE blend samples, observed using scanning electron microscopy (SEM) with different staining agents, explain their similarities and differences. There are two crops of rubber particles: larger ones belong to the original rubber crumbs that survived devulcanization; the smaller ones are fragments of partially DR. These crosslinked particles contribute to the overall degree of crosslinking in the blends. The devulcanized fractions of the DR materials are dispersed in the ACE matrix. Scattering at the interface accounts for the differences in the acoustic attenuation of the samples. © 2011 Wiley Periodicals, Inc. J Appl Polym Sci 124: 2062–2070, 2012

Key words: acoustic properties; ultrasonic detection; devulcanized rubber; styrene-butadiene-styrene copolymers; blend morphology

INTRODUCTION

The interactions of ultrasonic waves with their transport media in bulk and at the interfaces are very informational and have successfully been used for detecting defects in nondestructive testing and examination (NDT/NDE) for decades in both metal and nonmetal materials.[1–3] This has been especially successful in medical applications. Imaging techniques using ultrasonics are relatively recent developments building upon the advances of ultrasonic detector technologies and signal processing electronics. Applications of the ultrasonic technologies can also be found in food[4,5] and polymer processing.[6–11] Extrusion processes, one of the major polymer processing techniques, are monitored online by ultrasonic methods with respect to measurements of melt temperatures, and other applications include the development of foaming processes and tracking the degree of mixing during blending.

The changes in intrinsic ultrasonic properties of homopolymers are employed to sense the progress of a polymerization reaction. Ultrasonic waves were beamed through an epoxy curing system during reactive injection molding.[12] Based on the relationship between the acoustic properties and the degree of crosslinking in an epoxy resin, the progress of epoxy cure is quantified by the ultrasonic transmission or scattered signals.

The acoustic damping and attenuation properties of polymeric materials[13–15] are crucial to designers of ultrasonic instruments and equipment. Noise reduction and antidetection applications require materials of high acoustic attenuation or absorption. On the other hand, when maximum transmission of sonic waves is needed, the match of acoustic impedances between joining parts is crucial so as to allow minimum scattering or reflection of the sonic waves at the interfaces. Ultrasonic testing can also lead to inferences of other important material properties, namely rheological properties.[16,17] It can also be used to probe the compatibility of multiphase polymer blends and the emulsion droplet diameter and distribution. It is even possible to use specific phase structures in nanocomposites[18] or multiphase polymers as a filter to "tune" ultrasound waves to the desired purposes. The sonic velocity and attenuation

Correspondence to: A. Penlidis (penlidis@uwaterloo.ca).
Contract grant sponsor: Canada Research Chair (CRC).

properties can be related to the compatibility of the blend components in immiscible blends, e.g., polystyrene/poly(vinylmethylether)[19] and rubber blends.[20–22] Because of the differences in acoustic impedances between the phases and scattering at the curved interfaces in multiphase polymer blends or composites, the phase morphology will cause changes in acoustic attenuation.

Our aim in the current study is to characterize the degree of crosslinking in devulcanized rubber (DR) samples[23,24] obtained by a proprietary devulcanization process from commercially available tire rubber crumbs. The DR materials were thus blended with a styrene-butadiene-styrene (SBS) copolymer compound (referred to as ACE material or simply ACE in later sections) to yield a surface of good quality for acoustic testing. The acoustic properties of these blends were determined and the morphology of the blends was obtained using staining and scanning electron microscopy (SEM) techniques.[25–28]

EXPERIMENTAL

Sample compounding

Two devulcanized rubber samples (DR-10 and DR-30) were obtained from 10-mesh and 30-mesh rubber crumbs,[23,24] respectively, by extrusion devulcanization in the presence of supercritical carbon dioxide. They were dried and melt-blended with a styrene-butadiene-styrene block copolymer compound (ACE, Eclipse Scientific and MRI, Waterloo, Ontario, Canada) in a Haake mixer at 150°C for 15 min. Sixty parts by weight of ACE were mixed with 40 parts of DR materials. The rotor speed was 60 rpm. Specimens of different thicknesses were hot-pressed at 105°C for 10 min. using a stainless four-cavity mold. The four cavities had different depths, giving samples of different thicknesses in one molding step.

Mechanical testing

Specimens for tensile testing were press-molded on a hot-press at 105°C into a 2-mm-thick plate using a standard ASTM mold. Dumbell specimens were punched out of the plate from ASTM dies. The tensile properties were determined according to ASTM 420 on an Instron 3365 tester.

Staining and SEM

The samples were fractured after being rinsed in liquid nitrogen for 5 min. The fractured pieces were placed in a Petri dish. OsO4 or RuO4 drops were distributed in the dish but not in contact with the samples. The dish was covered and sealed by water to prevent the vapor from escaping. The fractured surfaces were exposed to OsO4 or RuO4 vapor for around 45 min and then placed on a sample holder for gold coating and scanning electron microscopy (SEM, Leo 1530) observation. Acceleration voltages used were 10 and 20 kV. Images were taken from a backscattering electron detector.

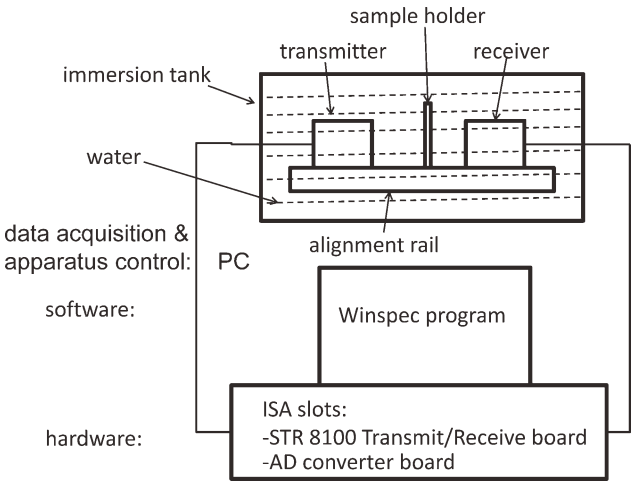

Figure 1 Schematic of the experimental set-up of the ultrasonic measurement apparatus.

Acoustic measurements

The acoustic measurements were conducted using a recently developed apparatus [Eclipse Scientific and Materials Research Institute (MRI), Waterloo, Ontario, Canada]. The apparatus, shown schematically in Figure 1, consists of an immersion tank (L200 × W50 × H40 mm) filled with deionized water and two ISA boards (STR 8100 A to D Pulse Echo Setup and Transmit/Receive Setup boards with PCPR 100 Pulser) installed inside a PC. In the immersion tank, a rail sits at the bottom and two ultrasound sensors (one emitter and one receiver, interchangeable) are mounted on two sliding blocks along the rail. A windowed sample mounting plate crosses the rail in the middle between the two detectors. The two detectors are connected by shielded cables to the ISA board (STR8100 A to D transmit/receive setup board and PCPR 100 Pulser), where ultrasonic signals are generated and received according to the control software Winspec. Figure 2 shows a screenshot of the work space in Winspec. The left side lower window is the PCPR-100 Pulser Setup Window which contains all the parameters controlling the pulse generation and detection. The right side window is an Ascan instrument display window, which displays the detected sonic pulses in time scale and Fast Fourier Transformed (FFT) frequency scale. The data can be saved into files shown in the right upper window. The pulse arrival time in the

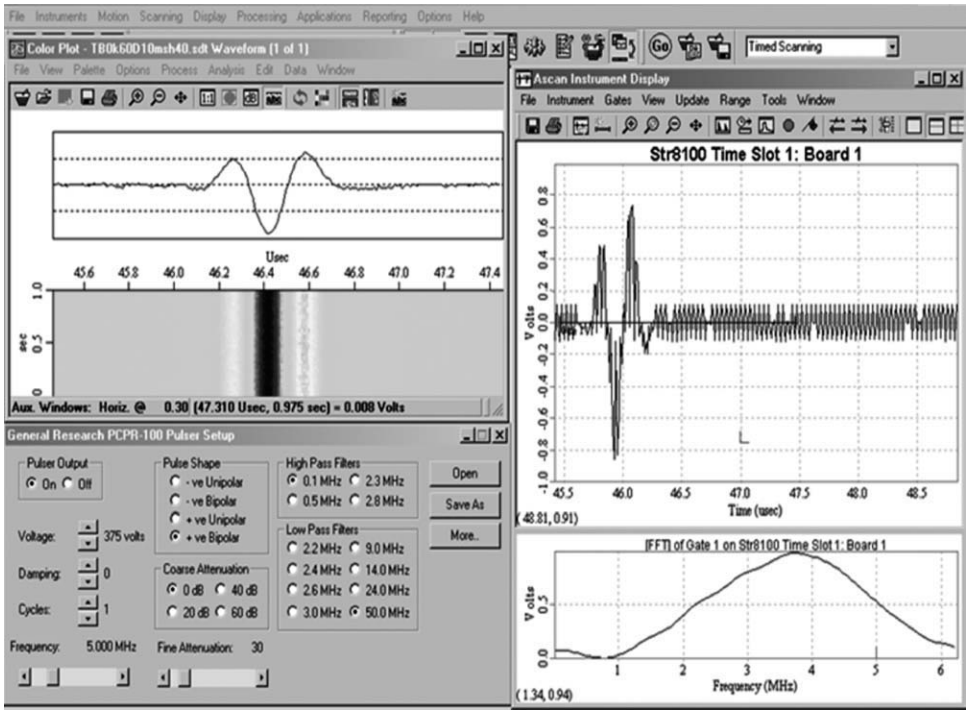

Figure 2 A screenshot of the workspace for the measurement of acoustic velocity and attenuation of the samples.

Ascan Instrument Display Window was recorded for the sonic speed measurements. The pulse amplitude in the same window was maintained at 80% by adjusting the coarse and fine attenuation slide in the PCPR-100 Pulser Setup Window in Figure 2. The values of the attenuation were recorded for the calculation of attenuation in the sample.

Samples with quality surface properties are very important because the reflection levels of ultrasound waves at the surface are dependent upon surface roughness. The pulse arrival time and the pulse amplitude readings are displayed in an Ascan Instrument Display Window (as shown in Fig. 2).

The velocity at which sound travels in the samples, V_s, is calculated by

$$V_s = \frac{d}{d - \Delta t \bullet V_w} V_w \tag{1}$$

where

V_w is the speed at which ultrasound travels in water (1500 m s^{-1});
d is sample thickness;
Δt is the difference in the pulse arrival time with and without sample.

The attenuation of the sample (Att, dB cm^{-1}) is obtained from the gain readings A and A_0 with and without the sample:

$$\text{Att} = \frac{1}{d} \cdot 20 \log\left(\frac{A_0}{A}\right) \tag{2}$$

where d is the thickness, and readings A and A_0 are the gain reading values (from the PCPR-100 Pulser Setup Window in Fig. 2) to maintain the pulse amplitude at 80% of the full scale (Ascan Instrument Display Window in Fig. 2) with (A) and without (A_0) samples in the path between the emitter and receiver ultrasonic sensors, respectively. The sample density was calculated from the weight and the volume measured from the sample dimensions.

RESULTS AND DISCUSSION

Table I gives the mechanical properties of the devulcanized rubber (DR) blends with 60 wt % of ACE material. Because the blends are not vulcanized, the strength is not very high, but the samples are tough to tear, and more importantly, the surface quality is appropriate for acoustic measurements, yielding reproducible results. The materials are very soft to the touch, with hardness levels below 40 Shore A. The differences between the two blends are not significant except for elongation-at-break. The elongation-at-break of the ACE/DR-30 blend is almost twice that of the ACE/DR-10 blend. The smaller elongation-at-break of the ACE/DR-10 blend likely originates from the larger particles (than in the

TABLE I
Mechanical Properties of 60/40 ACE/DR Blends

Samples		ACE/DR-30		ACE/DR-10		ACE	
		Average	SD	Average	SD	Average	SD
Hardness	Shore A	31.9	±1.0	39.8	±1.0	50.3	±1.4
Tensile strength	MPa	1.66	±0.1	1.37	±0.06	4.3	±1.7
Elongation-at-break	%	719	±73	437	±87	1103	±236
100% modulus	MPa	0.65	±0.01	0.97	±0.03	–	
300% modulus	MPa	1.15	±0.02	1.07	±0.62	–	
Tear strength	N mm^{-1}	13.2	±1.0	14.7	±1.0	22.2	±0.9

SD: standard deviation.

ACE/DR-30 blend), which survived the devulcanization process (see discussion below).

Acoustic properties

Ultrasound velocity

The sonic velocity in a medium can be measured either by the pulse-echo method[19,20] or transmission method, which was used in our case. The sonic velocity in the ACE/DR blend samples at four different thicknesses was determined using eq. (1). Figure 3 shows the ultrasonic velocity in ACE, ACE/DR-10 60/40 blend, and ACE/DR-30 60/40 blend samples versus thickness. For different samples, the values are very close to each other at each thickness, meaning that these three materials are very similar media for the ultrasonic waves to travel in. The three samples are indistinguishable in terms of ultrasound velocity. The sonic velocity in these media remains constant with sample thickness within a typical error of (or below) 5%.

Attenuation

Acoustic measurements in the pulse mode were conducted on the ACE and the two ACE/DR blend samples at different thicknesses. The ultrasonic attenuation levels (dB) in the ACE, ACE/DR-10 and ACE/DR-30 blend samples increase with thickness and exhibit different slopes as a function of thickness, as shown in Figure 4. The ACE material has the smallest value at all four thicknesses, while the ACE/DR-10 blend exhibits the highest levels of attenuation. To give a visual idea of the measurement error, two independently replicated measurements are shown for the ACE/DR-30 blend sample at the thickness of 2 mm.

The attenuation values in dB mm^{-1} for the three samples are shown in Figure 5. There are obviously three distinct levels, in agreement with Figure 4. Figure 6 shows the attenuation in dB mm^{-1} for the three samples versus their density. Three clusters of data points appear, which again indicate clearly different levels of ultrasound attenuation and density, and thus of sonic impedance z ($z = \rho \cdot v$, ρ: density; v: sonic velocity).

It is not surprising that the attenuations of both ACE/DR blend samples are much higher than those of the ACE sample. The rubber is only partially

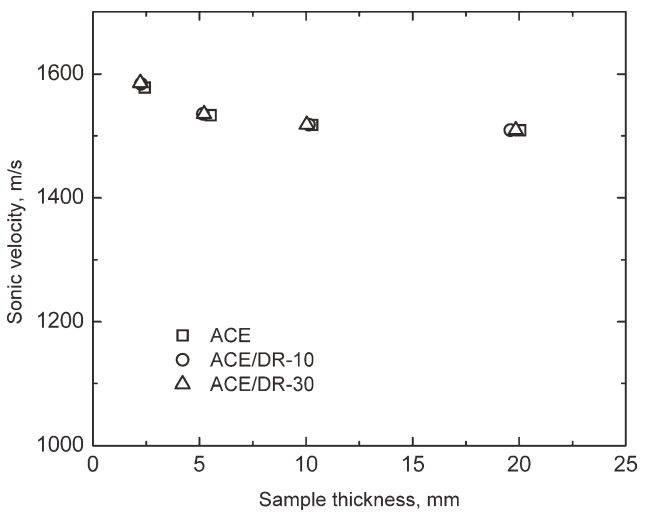

Figure 3 The velocity at which 5-MHz ultrasound travels in the samples as a function of sample thickness.

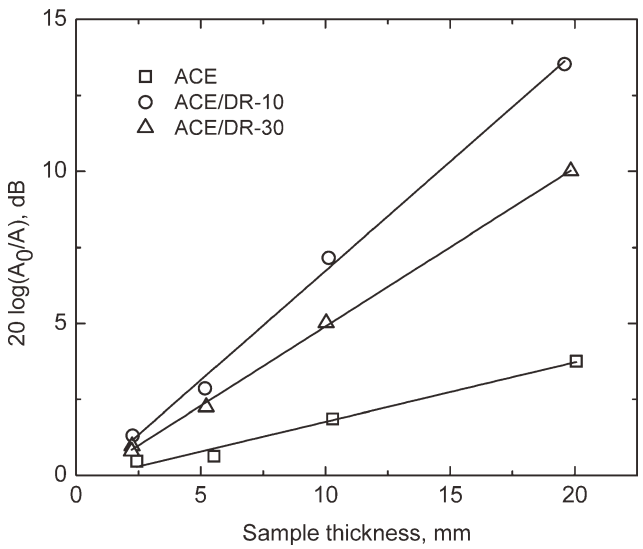

Figure 4 The attenuation level, $20\log\left(\frac{A_0}{A}\right)$, of 5-MHz ultrasound in the samples as a function of sample thickness.

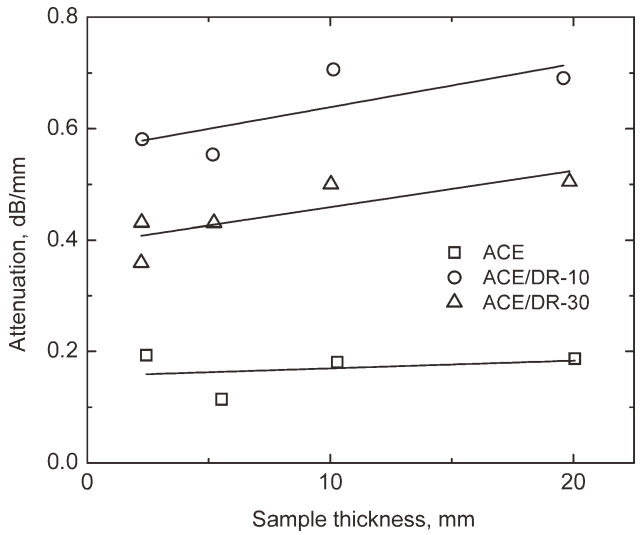

Figure 5 Ultrasound (5 MHz) attenuation (dB mm^{-1}) in the samples as a function of sample thickness.

devulcanized[23,24] and DR blends are expected to have a certain degree of remaining (residual) crosslinking, whereas the ACE material has no crosslinking. The ACE/DR-30 blend samples exhibit lower attenuation levels than the ACE/DR-10 samples. The residual degree of crosslinking in DR-30 is lower than that in DR-10 because the smaller size of the original rubber crumbs for DR-30 offers more surface area, and thus more devulcanization, than DR-10. This leads reasonably to a lower degree of residual crosslinking in the ACE/DR-30 blend sample than in the ACE/DR-10 sample.

Attenuation coefficient

The tone-burst mode was used to determine the attenuation coefficients for the two blend samples of different thicknesses. The gain (attenuation) values in the Pulser Window of Figure 2 were recorded and used in eq. (2), when the transmitted pulse amplitude was at 50% of the full scale (FS). The same values for water were also recorded for reference. A nominal 5-MHz probe was used and the tuned pulse frequency was adjusted to a frequency around 5 MHz. The sonic pulses which reached the detector showed multiple peaks on the frequency scale of the FFT plots. The transmitted frequency through the sample can be shifted to frequencies other than the incident frequency, but the main peak is still at the incident frequency. Figures 7 and 8 show the attenuation levels (dB) for the two blend samples at different sample thicknesses and incident ultrasonic frequencies. A thicker sample and a higher incident frequency lead to a higher level of attenuation, which is more pronounced for the ACE/DR-10 case.

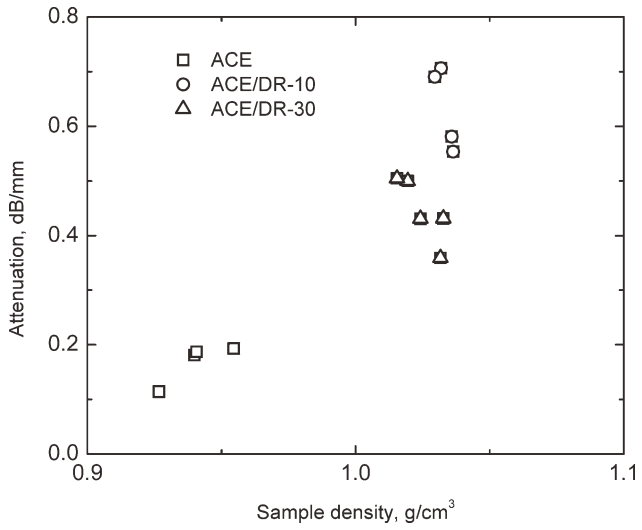

Figure 6 The attenuation (dB mm^{-1}) of the three samples as a function of specific density.

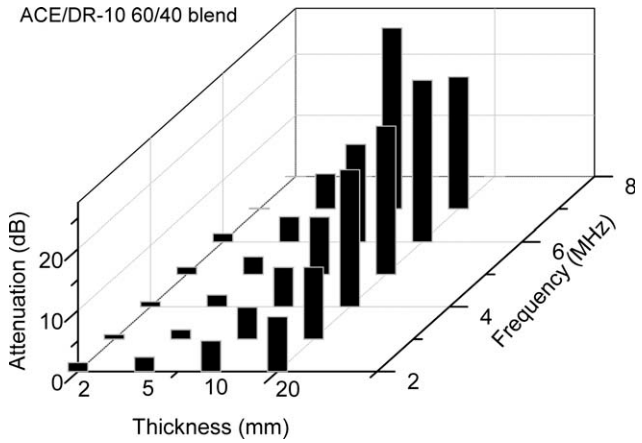

Figure 7 The attenuation levels (dB), $20\log\left(\frac{A_0}{A}\right)$, of 60/40 ACE/DR-10 blends at different specimen thickness and incident ultrasonic frequency.

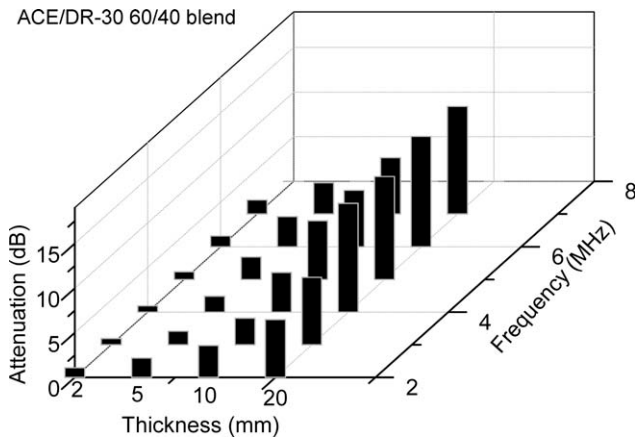

Figure 8 The attenuation levels (dB), $20\log\left(\frac{A_0}{A}\right)$, of 60/40 ACE/DR-30 blends at different specimen thickness and incident ultrasonic frequency.

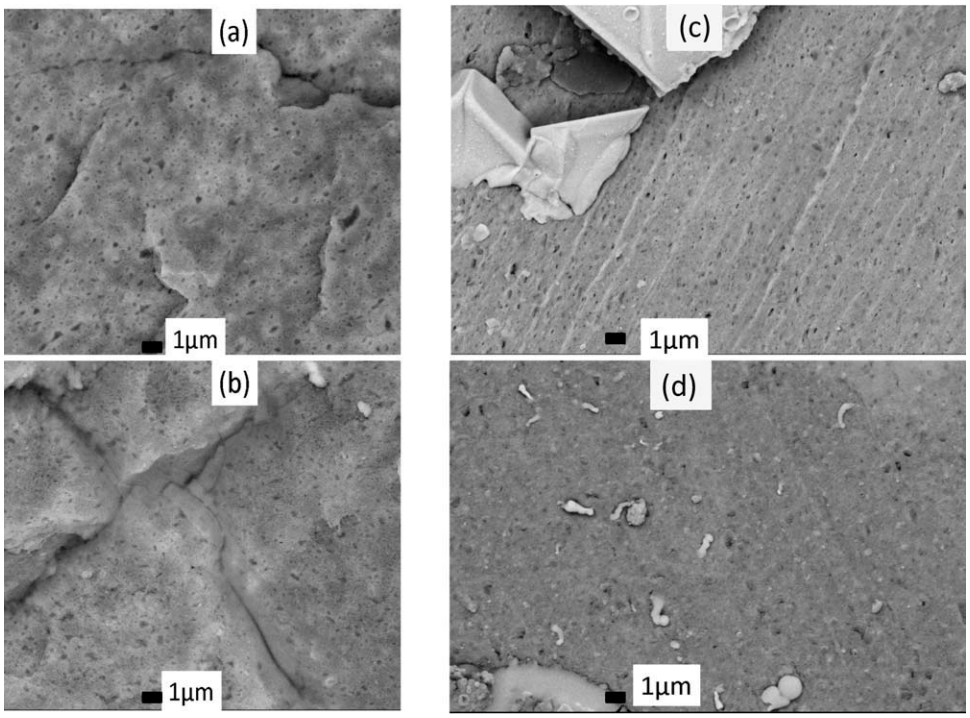

Figure 9 SEM micrographs of cryo-fractured surfaces of ACE sample under 20 kV (a, b) and 10 kV (c, d) stained with OsO4 (a, c) and with both OsO4 and RuO4 (b, d).

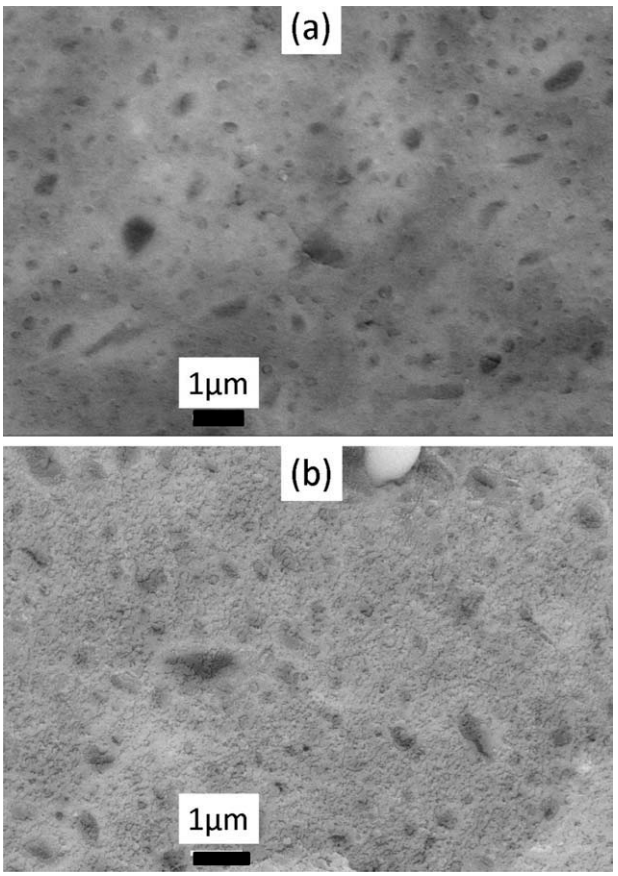

Figure 10 High-magnification SEM micrographs under a voltage of 20 kV of cryo-fractured surfaces of ACE sample stained with (a) OsO4; (b) OsO4 and RuO4.

Morphological analysis

The phase structure of ACE samples

Figure 9 shows the morphology of the ACE samples stained by OsO4 as well as by OsO4 and RuO4. The two staining agents were used to reveal the different structures in the material. The ACE material shows clearly as a two-phase-structured polymer under the SEM microscope after staining with OsO4 [Fig. 9(a)], since it is a blend of styrene-butadiene-styrene (SBS) copolymer and a polyolefin. The bright matrix is mainly butadiene stained with OsO4, while the dark dispersed "spots" are likely composed of polystyrene- and polyolefin-rich material, which cannot be stained by OsO4. The particle size is below 1 µm. After both RuO4 and OsO4 staining [Fig. 9(b)], the phase structure appears to be the same, but the contrast between the two phases is less pronounced than that with OsO4 staining only [Fig. 9(a)]. This reduction in the contrast by RuO4 staining is observed visually at a higher magnification (Fig. 10). The reason for this may lie in the fact that RuO4 can readily stain the polystyrene and other amorphous saturated polyolefins, in addition to the rubbery parts with double bonds, thus reducing the contrast between the brighter rubber phase and the polyethylene/polystyrene phase. A worm-like bright "cylinder" can be observed on the RuO4-stained surfaces. This is believed to be the other component (polyolefin) in the SBS compound.

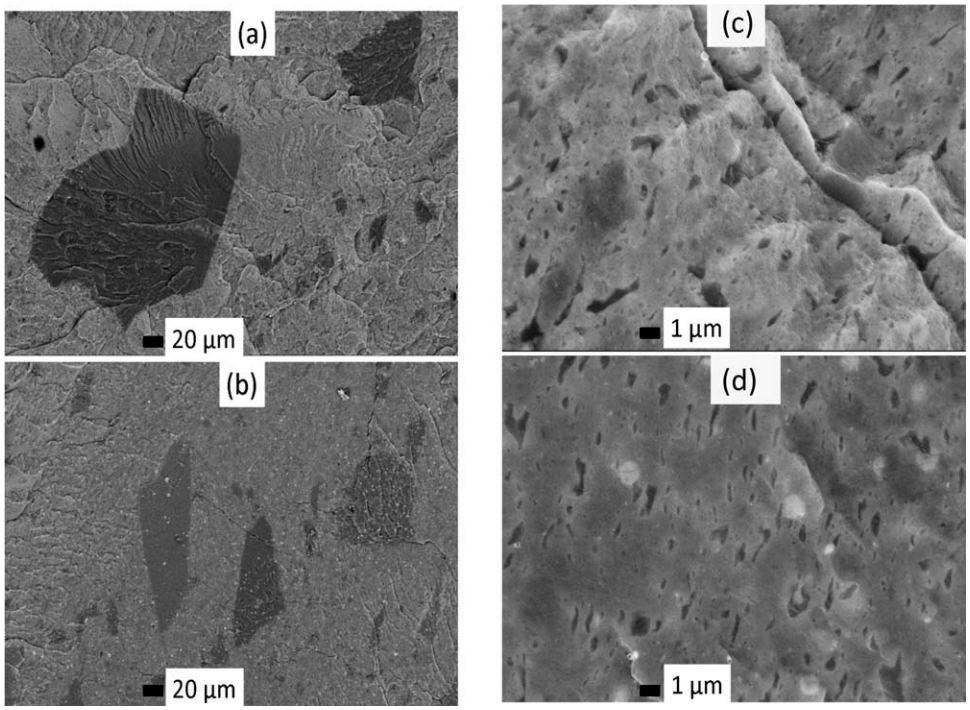

Figure 11 SEM micrographs of cryo-fractured surfaces of ACE/DR (a,c: DR-10; b, d: DR-30) sample at a lower (a, b) and a higher magnification (c, d) stained with OsO4.

It is known that lower SEM accelerating voltage decreases the contrast between the phases in its image, especially in the backscatter electron image. Figure 9(c,d) show the SEM micrographs of the ACE samples with a lower accelerating voltage (10 kV) than in Figure 9(a,b) as well as Figure 10 (20 kV). The two-phase structure is barely observed in OsO4 stained samples [Fig. 9(c)], and is almost undistinguishable in the sample stained with both OsO4 and RuO4 [Fig. 9(d)], where the worm-like polyolefin block in SBS shows up again.

Phase structures of ACE/DR blends

Figure 11(a,b) show SEM micrographs of 60/40 ACE/DR blends at a very low magnification, thus the largest particles can be observed in whole. The sample surfaces were stained with OsO4, and the images were taken at an accelerating voltage of 20 kV from a backscatter electron detector. The darkest and largest particles in both images take the irregular shapes from the original rubber crumbs before devulcanization. This suggests that a small fraction of rubber crumbs survived the devulcanization process without being fragmented or deformed on the skin layer. The 30-mesh rubber crumbs, which were devulcanized to produce DR-30, are smaller and appear to be lighter than the 10-mesh rubber crumbs in the ACE/DR-10 blend. Both rubber crumbs are darker than the SBS matrix, in which the butadiene component, easily stained by OsO4, may have a higher density of double bonds than the rubber crumbs.

At a higher magnification [Fig. 11(c,d)], the dark particles in the range of 1–10 μm are noticeably different from the submicron particles, as also observed in the ACE samples in Figures 9–10. These particles are attributed to the fragmented rubber particles by the devulcanization process. Because the sample now contains styrene–butadiene copolymer, the fragmented rubber may merge into the polyethylene/polystyrene-rich phase in ACE, and expand the dispersion size above the microscale. It is noteworthy that the ACE/DR-30 blend appears to have a third phase-dispersion, mostly spherical, brighter than the matrix. The brightness suggests that the third phase consists of a component with a higher density of double bonds, which may come from the devulcanization process. This third component is absent in the ACE/DR-10 blends. The devulcanization of 10-mesh rubber crumbs has not produced enough of the same component to form a third phase in the ACE/DR-10 blend.

Figure 12 presents the boundary areas near the rubber crumb particles for the two blend samples. Excellent adhesion between the particle and the matrix phases obscures the location of the boundaries. The third phase is not only in the matrix but also on the rubber crumb particles. This third phase seems to attach to the particles during devulcanization or the blending process.

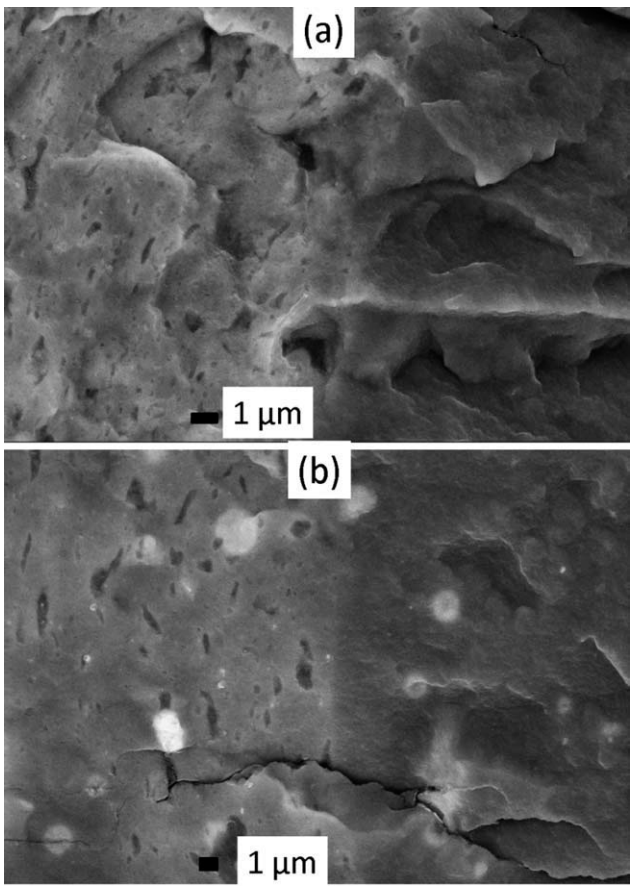

Figure 12 High-magnification SEM micrographs of the interfacial regions on cryo-fractured surfaces of ACE/DR (a: DR-10; b: DR-30) sample stained with OsO4.

The two crops of rubber particles found in the two blends represent the fraction of undevulcanized rubber. According to extraction measurements of DR materials,[23,24] the undevulcanized or insoluble fraction in the DR accounts for ~ 30–40%. Thus the volume fraction of the rubber particles in the OsO4 stained images is expected to be around ~ 15%, which appears to agree with the micrographs shown in Figures 11 and 12. The devulcanized (soluble) fraction is homogeneously dispersed in the matrix.

Figure 13(a,b) show the SEM micrographs of the two blends stained by both OsO4 and RuO4. The worm-like structures are observed again in the ACE/DR-30 blend. The very large rubber crumbs (which survived devulcanization) in the blends appear brighter than the matrix [Fig. 13(b)], suggesting that the rubber crumbs can be stained more by RuO4 than by OsO4. This is probably due to the presence of polystyrene which is reactive with RuO4. However, the fine phase structures in the OsO4-stained samples are completely obscured by the subsequent RuO4 staining.

At a lower accelerating voltage of 10 kV [Fig. 13(c,d)], the surfaces of OsO4-stained samples show only the two phases of SBS and the rubber particles because of shallower (i.e., diminished) contrast.

Further discussion

The attenuation of acoustic waves in solids consists of the classic attenuation, which includes absorption

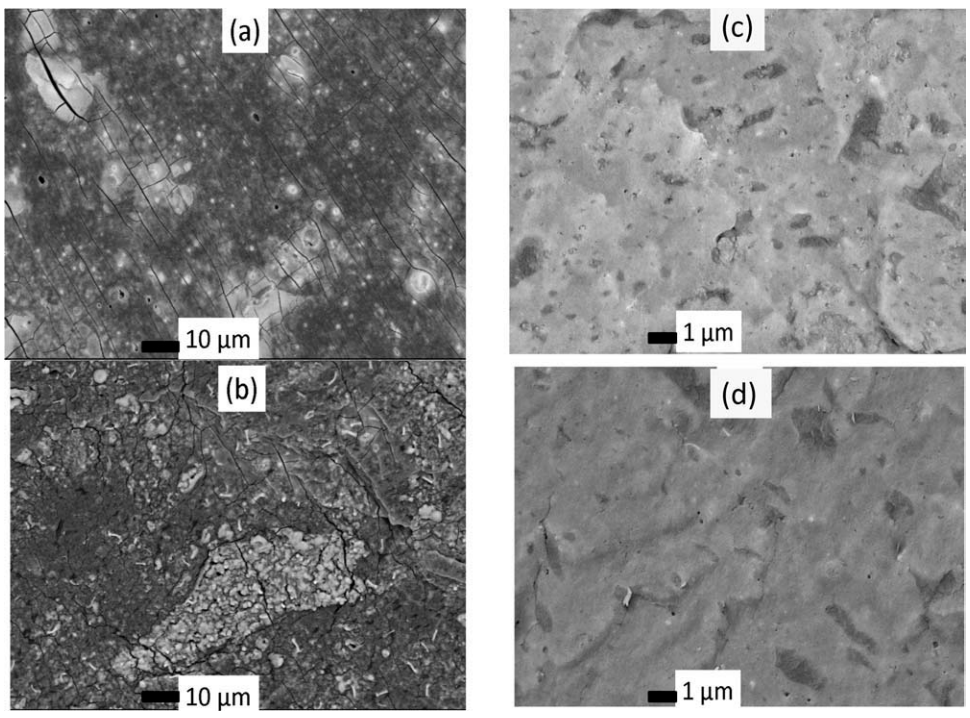

Figure 13 SEM micrographs under 20 kV (a,b) and 10 kV (c, d) of cryo-fractured surfaces of ACE/DR (a, c: DR-10; b, d: DR-30) sample stained with both OsO4 and RuO4.

attenuation and scattering attenuation between layers. The attenuation (Att, dB cm^{-1}) of sonic waves in a medium of thickness d can be determined according to eq. (3).

$$\mathrm{Att} = \frac{1}{d} \cdot 10 \log \frac{\int_0^\infty [v_1(t)]^2 dt}{\int_0^\infty [v_2(t)]^2 dt} - 20 \log \frac{4 z_1 z_2}{(z_1 + z_2)^2} \qquad (3)$$

The second term in eq. (3) is the corrected transmission loss between the media, and z_1 and z_2 are their acoustic impedance values on both sides of a boundary. The energy signals v_1 and v_2 are replaced by the pulse amplitudes during measurements, and hence eq. (3) becomes eq. (4).

$$\mathrm{Att} = \frac{1}{d} \cdot 20 \log \frac{A_0}{A} - 20 \log \frac{4 z_1 z_2}{(z_1 + z_2)^2} \qquad (4)$$

The second term in eq. (4) will not have an effect, if samples of gradually increasing thickness are used, and hence eq. (2) can be used to determine attenuation. In fact, the second term in eq. (4) can be used for multiphase materials at the curved interfaces between the dispersed phase and the main matrix. The term, $\frac{4 z_1 z_2}{(z_1+z_2)^2}$, is the transmission coefficient. The larger the differences in the acoustic impedances between the phases, the less the sonic waves pass through the interface. Instead, they will be scattered at the interface, causing even more attenuation. A larger interface area will lead to more vigorous attenuation. Only when the difference disappears (i.e., $z_1 = z_2$), then the sonic waves can pass through the media directly with minimum attenuation.

Good contrast between the phases in the blends means different densities of double bonds with respect to the SBS phase, which points to different degree of crosslinking or devulcanization in the DR phases. This different degree of crosslinking in the DR phases will result in different absorption attenuation. The attenuation can thus be used as an indicator for the degree of devulcanization.

CONCLUSIONS

The morphologies of both ACE/DR-10 and ACE/DR-30 blends show that there are two crops of rubber particles dispersed in the ACE phase. The large irregular-sized particles are rubber crumbs which survived the devulcanization process, while the small, spherical-sized ones belong to fragments that are partially devulcanized. The devulcanized fraction is dispersed in the ACE matrix. The amount of this devulcanized fraction is enough to form yet a third phase in the ACE/DR-30 blend, which is absent in the ACE/DR-10 blend. The acoustic properties of ACE/DR-10 and ACE/DR-30 blends show significant differences in attenuation, although ultrasonic speeds appear to be the same in both media. This difference arises from the residual degrees of crosslinking in DR-10 and DR-30, i.e., the differing degree of devulcanization.

Donation of the ultrasonic measurement apparatus and interactions with MRI and Eclipse Scientific, both of Waterloo, ON, Canada, are greatly appreciated.

References

1. Ensminger, D. Ultrasonics—The Low- and High-Intensity Applications; Marcel Dekker: NY, 1973.
2. Krautkramer, J.; Krautkramer, H. Ultrasonic Testing of Materials; Springer: Berlin, 1990.
3. Ensminger, D. Ultrasonics—Fundamentals, Technology, Applications, 2nd ed.; Marcel Dekker: NY, 1988.
4. Shukla, A.; Prakash, A.; Rohani, S. Non-Destructive Techn. Conf. Paper; ACS: London, 2009.
5. Sahnoune, A.; Tatibouet, J.; Gendron, R.; Hamel, A.; Piche, L. J Cell Plast 2001, 37, 429.
6. Shen, J.; Edwards, R.; Thomas, C. L.; Bur, A. J. ANTEC Proc 1998, 2, 2076.
7. Cobb, W. N.; Johson, J. J. Ultrasonic Proc IEEE Ultrasonics Symp 2001, 1, 733.
8. Franca, D. R.; Jen, C.-K.; Nguyen, K. T.; Gendron, R. Polym Eng Sci 2000, 40, 82.
9. Chen, T.-F.; Nguyen, K. T.; Wen, S.-S. L.; Chen, C.-K. Meas Sci Technol 1999, 10, 139.
10. Wen, S.-S. L.; Chen, T.-F.; Romas, F. D.; Nguyen, K. T.; Chen, C.-K.; Ihara, I.; Derdouri, A.; Garcia-Rejon, A. Proc SPIE Intern Soc Opt Eng 1998, 3399, 122.
11. Gendron, R.; Daigneault, L. E.; Tatibouet, J.; Dumoulin, M. M. ANTEC Proc 1994, 1, 167.
12. Contable, G. S.; Lesser, A. J.; Coughlin, E. B. J Polym Sci B 2003, 41, 1323.
13. Yao, K.; Cheng, G.; Liu, T.; Zhu, W.; Shun, Q.; Wang, T. J Appl Sci 1995, 58, 565.
14. Asdrubali, F.; Pispola, G. J Acoust Soc Am 2000, 121, 214.
15. Burke, M.; Townend, D. J Plast Rubber Comp 1999, 28, 185.
16. Jung, S. S.; Kim, Y. T.; Lee, Y.-B.; Shin, S. H.; Kim, D.; Kim, H. C. J Korean Phys Soc 2006, 49, 1961.
17. Graciert, C.; Hosten, B. IEEE Ultrasonics Symp 1994, 1, 1219.
18. Tiefensee, F.; Becker-Willinger, C.; Heppe, G.; Herbeck-Engel, P.; Jakob, A. Ultrasonics 2010, 50, 363.
19. Hourston, D. J.; Hughes, I. D. Polymer 1978, 19, 1181.
20. Thomas, G. V.; Gopinathan Nair, M. R. J Appl Polym Sci 1998, 69, 785.
21. Singh, P.; Singh, R. P. Eur Polym Mater 1984, 20, 201.
22. Sidkey, M. A.; Abd El Fattah, A. M.; Yehia, A. A.; Abd El, A. N. S. J Appl Polym Sci 1991, 43, 1441.
23. Zhang, Q.; Tzoganakis, C. ANTEC Proc 2004, 1, 3509.
24. Tzoganakis, C. Method. US Patent 7,189,762, 2002.
25. Buschnakowski, M.; Adhikari, R.; Michler, G. H.; Knoll, K. J Appl Polym Sci 2007, 106, 1939.
26. Goizueta, G.; Chiba, T.; Inoue, T. Polymer 1993, 34, 253.
27. Sano, H.; Usami, T.; Nakagawa, H. Polymer 1986, 27, 1497.
28. Trent, J. S.; Scheinbeim, J. I.; Couchman, P. R. Macromolecules 1983, 16, 589.